Rijksuniversiteit Groningen

Bachelor Thesis

Hydrocarbons in Protoplanetary Disks

Evaluating the carbon to oxygen ratios in protoplanetary disks

Author:
P.S. Hartog

Supervisor:
prof. dr. I.I.E. Kamp
J. Kanwar

Abstract

Context: Protoplanetary disks form around newborn stars and provide the region in space for planets to form. Since their environment is what planets form from, exploring the chemistry occurring there is key to our understanding of planet formation and evolution. It has often been suggested that the carbon to oxygen ratio in these disks is well above the solar value, which would lead to carbon based chemistry and thus also carbon rich planets forming in these regions.

Aims: This thesis aims to evaluate the C/O ratio in the outer regions of protoplanetary disks to see if an elevated value is indeed necessary to explain the current ALMA observations of, for example, hydrocarbons in the disks.

Methods: Two of the more commonly observed hydrocarbons, C_2H and C_3H_2, are chosen in the observations made by the MAPS project and compared to simulated disk models. These models are set up at two C/O ratios, using ProDiMo, allowing for the C/O ratio in the disks to be evaluated.

Results The solar C/O models' integrated line fluxes more closely approach the MAPS observed fluxes. For the radial intensity profiles, the C/O ratio had very little effect on reproducing the MAPS observations. From the column densities no C/O ratio should be concluded as they are derived values rather than direct observables.

Conclusions: The observations of protoplanetary disks can be reproduced with a C/O ratio well below the value of 2 suggested by the MAPS team. This implies that the processes responsible for creating the enhanced C/O ratios may not be as prevalent in the disk as previously thought. Derived quantities from models, like column densities, are better suited to comparing the underlying processes that drive the models.

Acknowledgements

This thesis would not have been possible without the guidance and insights of my supervisors Dr. Inga Kamp and Jayatee Kanwar. Their ability to answer all my questions and help in guiding me through my first real attempt at scientific research has been invaluable and I cannot thank them enough.

I would also like to thank the SPFE group for welcoming me to the meetings every Friday, piquing my interest in research regarding exo-planets and their formation and providing feedback to improve the presentation of this thesis.

Additionally, I would like to thank my friends at the Kapteyn Institute and Energy Academy for their company the past three months and making them some of the best of my Bachelors degree. Finally, a big thank you to my parents and sister for always being willing to help me out with this thesis, despite it not being within their own areas of expertise.

Contents

1 Introduction

Protoplanetary disks are some of the most interesting regions of space. These large, flattened disks around newly formed stars are the birthplace of objects like planets, asteroids and comets. With the exoplanet field of study continuing to evolve thanks to telescopes such as JWST, see, for example, the recent paper by Madhusudhan et al. (2023), it is also important to understand the regions of space where these exoplanets form, namely the protoplanetary disks. The type of chemistry that occurs in these disks determines the types of planet that form. Thus investigating what molecules are present in the disks and the processes they go through is vital to our understanding of exoplanets and their formation.

Of course, observing these disks is easier said than done. Observatories like ALMA can observe the emission spectra of disks and the intensity of these spectra, but extracting things like substructures and abundances of the molecules has to be done based on models. Because of the computations involved with this, there is quite some debate on, for example, the carbon and oxygen abundances in planet-forming disks. Like Le Gal et al. (2021), who suggest a carbon to oxygen ratio (C/O) of at least 0.9 in the disk, well above the solar carbon to oxygen ratio. While others, like Alarcón et al. (2021), suggest locally increasing the C/O ratio up to 2, before it drops back down to solar levels further out in the disk.

To study these molecular abundances in more detail, it can be incredibly useful to a create high resolution computer model, which can take in specific C/O ratios as input and then solve the chemical processes in the disks. By comparing these models to the observations, the precise values of the C/O ratio in protoplanetary disks can be examined. Furthermore, the necessity of certain processes needed to produce an enhanced C/O ratio can also be determined.

1.1 Protoplanetary Disks

1.1.1 Pre-Main Sequence Stars

Planet-forming disks are formed in the early stages of a star's life, before it becomes a main sequence star in its hydrogen-burning phase. Therefore it is prudent to have definitions for the types of pre-main sequence stars, which can typically be divided into Herbig Ae/Be or T Tauri stars based on their mass. Of the two, Herbig Ae/Be stars and their disks will be the focus of this thesis. Based on the original observations by Herbig (1960), Waters and Waelkens (1998) describe three defining characteristics of Herbig Ae/Be stars:

1. "spectral type A or B with emission lines"
2. "infrared excess due to hot or cool circumstellar dust or both"
3. "luminosity class III to V"

The masses of Herbig Ae/Be stars are between 2 and 10 $M_{\odot}$ (Wichittanakom et al., 2020).

1.1.2 Disk Formation

Stars form through the gravitational collapse of a slowly rotating molecular cloud. As described by Dominik (2015), when such a spherical cloud collapses, due to angular momentum conservation, gas parcels can either accrete onto the protostellar core or onto an equatorial disk. The outcome of this collapse is an outer envelope that stays spherical, an inner region that is distorted by rotation to form this equatorial disk and, of course, the pre-main sequence star (Dominik, 2015).

After about 1 Myr the envelope will have completely dispersed, leaving only the star and the disk, which can now be described as protoplanetary, rather than protostellar. From this point, the disk evolves through, for example, accretion onto the star and agglomeration into larger bodies like planets (Williams and Cieza, 2011).

The typical lifetime of these disks is 2 to 3 Myr, but can range from less than 1 Myr in low metallicity environments to 10 Myr around very low-mass stars or brown dwarves (Williams and Cieza, 2011).

Since I will be focusing on the outer protoplanetary disks, it should be noted that the inner and outer regions of these disks are separated by the snowline of water (Öberg et al., 2023). Here the ice line of a molecule, snowline for water specifically, is the point at which the molecule freezes out from a gaseous to solid phase.

1.1.3 Morphology

Through observations of optical or infrared scattered light and mm continuum emission, high resolution images can be made that show the substructure of the dust in protoplanetary disks. With those images, the morphology of the disks can be categorised. Andrews (2020) identifies the following four categories, which I will also be using:

- **Ring/Cavity**: the disk consists of a primary ring, encircling a cavity, as shown in panel a of Figure 1.

- **Ring/Gaps**: the disk shows a pattern of concentric, axisymmetric rings and gaps, as shown in panel b of Figure 1.

- **Arcs**: there is an asymmetric substructure to the disk. For example, a partial ring or an additional substructure outside of the ring/gap morphology, as shown in panel c of Figure 1.

- **Spirals**: disks with spirals are usually 2 armed spirals, that range from relatively open to more complex and tightly wound, as shown in panel d of Figure 1.

It should, of course, be noted that some disks cannot be categorised as a single morphology, but rather show characteristics of multiple types.

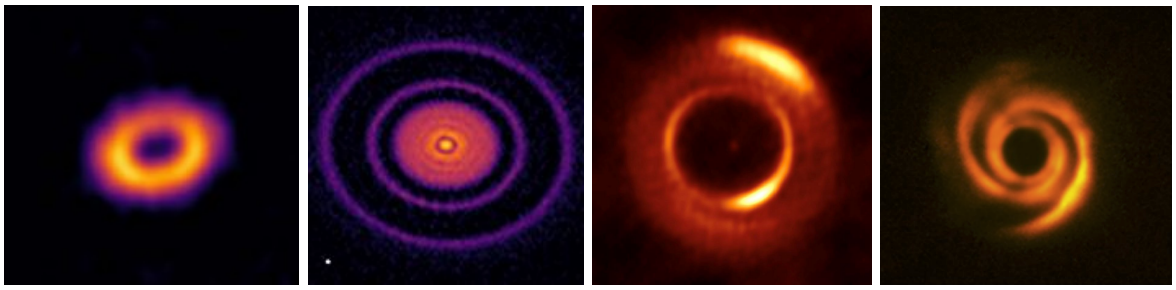

Figure 1: Protoplanetary disk structures. From left to right; *panel a*: ring/cavity disk CIDA 9 (Long et al., 2018), *panel b*: ring/gaps disk AS 209 (Andrews et al., 2018), *panel c*: arcs disk MWC 758 (Dong et al., 2018), *panel d*: spiral disk HD 135344B (Stolker et al., 2016)

.

1.1.4 Disk Chemistry and C/O Ratios

In Öberg et al. (2023) the chemical composition of a protoplanetary disk is determined by both inheritance and in situ chemistry. This means that, for example, elemental ratios can differ from stellar values. Furthermore, the chemical, physical and dynamical processes in disks are closely linked, so combining observations of these individual processes, allows us to probe aspects of disk evolution and planet formation. Some of the chemical processes occurring in disks include, ice sublimation, grain surface (photo) chemistry and gas-phase (photo) chemistry. Figure 2 shows an overview of some of the major chemical processes and where they occur in protoplanetary disks. (Sub)mm observations can give us spectroscopic characterisations of the cold gas and the rotational transitions of molecules in the disk, allowing us to study these chemical processes.

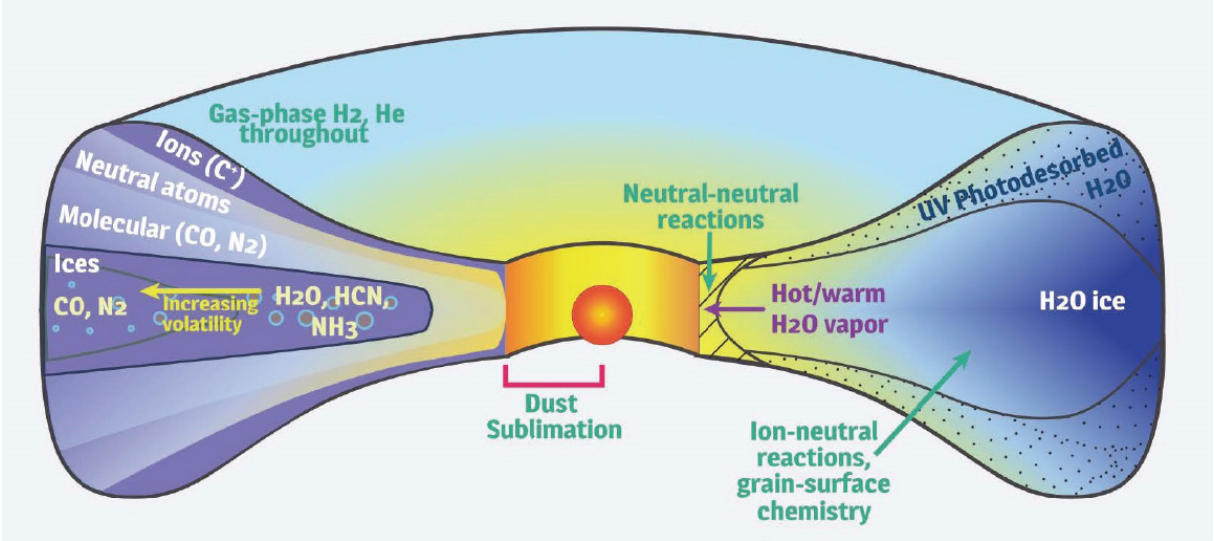

Figure 2: Overview of the chemical processes in protoplanetary disk, from Cleeves (2018).

As mentioned earlier, an important variable to disk chemistry is the carbon to oxygen (C/O) ratio. As first suggested by Öberg et al. (2011) the C/O ratio in a planetary disk can change, depending on the distance to the star due to ice lines. Thus the C/O ratio of an exoplanetary atmosphere can be used to gauge where the planet formed in the disk. But in order to make those calculations reliable, the precise C/O ratios in the protoplanetary disks need to be known and so they need to be studied. Two of the most important molecules for that are H_2O and CO, as those are the main carriers of oxygen and carbon, respectively, in protoplanetary disks. Unfortunately, due to the high abundance of water in Earth's atmosphere, observing H_2O in the disks becomes very difficult. Even for telescopes like ALMA, which are at high and dry sites, it is only possible in some cases to observe water isotopes. However, other options for deriving the C/O value exist with papers like Bosman et al. (2021) basing their C/O estimate of 2 on hydrocarbons column densities, such as C_2H.

1.1.5 Vertical Cold Finger Effect

To explain molecular observations of protoplanetary disks, supersolar C/O values are often found to be necessary within protoplanetary disks, like in Le Gal et al. (2021) and Alarcón et al. (2021). Importantly, these enhanced C/O ratios are only for the disk and not the star it surrounds. Hence, there need to be some additional processes that can create the enhanced C/O value.

One of the leading processes for this is the so-called vertical cold finger effect, as illustrated

in Figure 3 and described by Meijerink et al. (2009). Due to temperature inversion in the disk atmosphere, molecular ice lines become almost parallel to the disk midplane in the outer parts of the disk. Along these radial ice lines, vertical turbulence in the gas leads to a cold finger effect in the vertical direction. In this vertical cold finger effect, H_2O vapour is moved below the ice line by the aforementioned turbulence. The H_2O promptly freezes out onto dust grains which settle subsequently to the disk's midplane, taking the H_2O ice along with it. These dust grains eventually become too heavy, from the gathered ice and collisional growth, for the turbulence to transport them back up above the ice line, leaving the gas high up in the disk depleted of H_2O and thus oxygen in general (Meijerink et al., 2009). Numerical simulations like the one by Krijt et al. (2016) show the validity of this vertical transport and that in order to achieve enhanced C/O ratios, effects like this need to be taken into account. Since the vertical cold finger effect affects the main carrier of oxygen, H_2O, the oxygen in the disk gets depleted and the gas obtains a high C/O ratio.

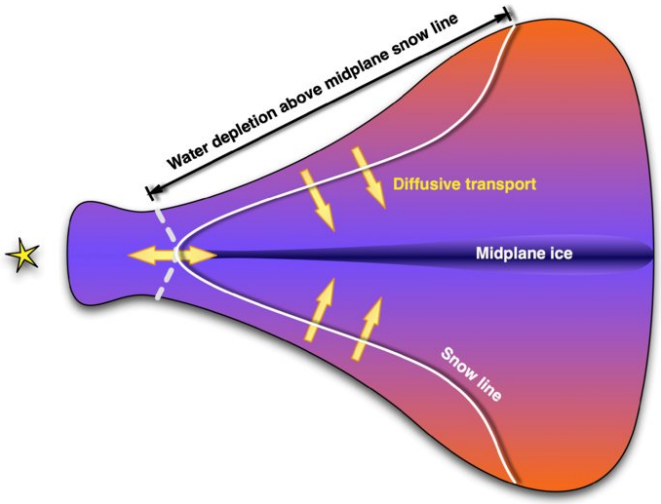

Figure 3: Diagram of the cold finger effect (Meijerink et al., 2009)

1.1.6 Planet Formation

The process of planet formation is complex and somewhat beyond the scope of this thesis so this will only be a brief description and for more a complete explanation I refer to references, like the reviews by Lissauer (1993) or Johansen et al. (2014).

The gas C/O ratio in a disk mainly affects gas giant planets, forming in the outer regions of the disk. Hence I provide a short summary of the process behind the formation of gas giants. This begins with dust grains in the protoplanetary disk accreting into larger planetesimals. Once these planetesimals are large enough, runaway growth can occur to form the terrestrial planets and cores of giant planets. Through rapid gas accretion the giant planets cores can grow to Jupiter masses (Helled et al., 2014).

With giant planets like WASP-12b being observed to have a C/O ratio over 1 in its atmosphere (Madhusudhan et al., 2011), the gas C/O ratio in the disk where the planet formed, and thus accreted by the planet to form its atmosphere, becomes important to understanding the properties and formation of exoplanets. Bergin et al. (2024), for example, explored the effect of elevated C/O ratios in the protoplanetary disk's gas on planet formation and why the exoplanetary atmospheres that have been directly observed so far do not seem to have an equally elevated C/O ratio.

1.1.7 ProDiMo

In this thesis, I will use a computer model to study the protoplanetary disks in detail. More specifically, I will use the thermo-chemical model ProDiMo, standing for Protoplanetary Disk Model (Woitke et al., 2009; Kamp et al., 2010; Thi et al., 2011) and which calculates the physical, thermal and chemical structure of protoplanetary disks.

Parameters used as input are fully listed in Table 7 of Woitke et al. (2019) and include stellar mass, luminosity and effective temperature of the star, disk inner and outer radii, disk gas and dust mass and disk scale height. The standard ProDiMo model parameters were defined by Woitke et al. (2016), where the impact of each parameter on the disk model was also explored. The chemical network in the models is based on the DIANA network as described by Kamp et al. (2017) and importantly to this thesis, the hydrocarbon network in the model, has been expanded upon by Kanwar et al. (2024) to include species of up to eight carbons long. Once set up, ProDiMo uses 2D dust continuum radiative transfer, gas phase and photochemistry, ice formation, heating and cooling balance and the vertical disk structure to provide detailed descriptions of the protoplanetary disks (Woitke et al., 2009). This includes gas abundances, line origins and column densities.

1.1.8 Disks Studied in this Thesis

- MWC 480

The first disk I will discuss is the one around the Herbig Ae star MWC 480, for convenience I will also refer to the disk as MWC 480. Liu et al. (2019) find that the disk contains small grains, with radii between 0.01 and 2 μm, up to a radius of 750 au and estimate a disk gas mass between 0.008 and 0.16 $M_\odot$. High resolution images, like from Parker et al. (2022), show a disk that has a single gap, placing the disk in the disk/cavity category. This gap can potentially be explained by a planet, which Liu et al. (2019) suggest to have a mass of 2.3 M_J at a radius of 78 au. A continuum image at 1.33 mm by Long et al. (2018) in the left panel of Figure 4 shows this structure.

- HD 163296

The other disk I will study is the disk around the Herbig Ae star HD 163296, which I will, again, use to refer to the disk as well. It extends to a radius of 1000 au from the star and has a mass between 0.01 and 0.15 $M_\odot$ (Isella et al., 2018). Parker et al. (2022), among others, found the disk to have rings in its structure, placing it in the ring/gaps category. According to Isella et al. (2018) these rings are also created by, as of yet, unseen planets and their gravitational interactions with the disk. The DSHARP program (Andrews et al., 2018) has observed HD 163296 at high resolution at 1.25 mm wavelength, as shown in the continuum image in the right panel of Figure 4. Furthermore, both HD 163296 and MWC 480 are not obstructed by cloud material nor do they have envelope emission substantial enough to complicate line observations, making them prime observation targets for molecular studies (Öberg et al., 2021).

Since these disks are such good observation candidates, they are well-studied, including studies where their C/O ratios were determined. Bosman et al. (2021), for example, uses C_2H column densities to derive C/O ratios for both these disks. They find that, for HD 163296, the C/O ratio is approximately 2 beyond 50 au, but that in the inner 20 au the C/O is solar. For MWC 480, they also find a C/O ratio of approximately 2, but this time with a peak at 70 au and again, within the inner 20 au the C/O is approximately solar. Appendix C in Bergin et al. (2024) also provides a clear summary of previous literature on the C/O values in these two disks. Other

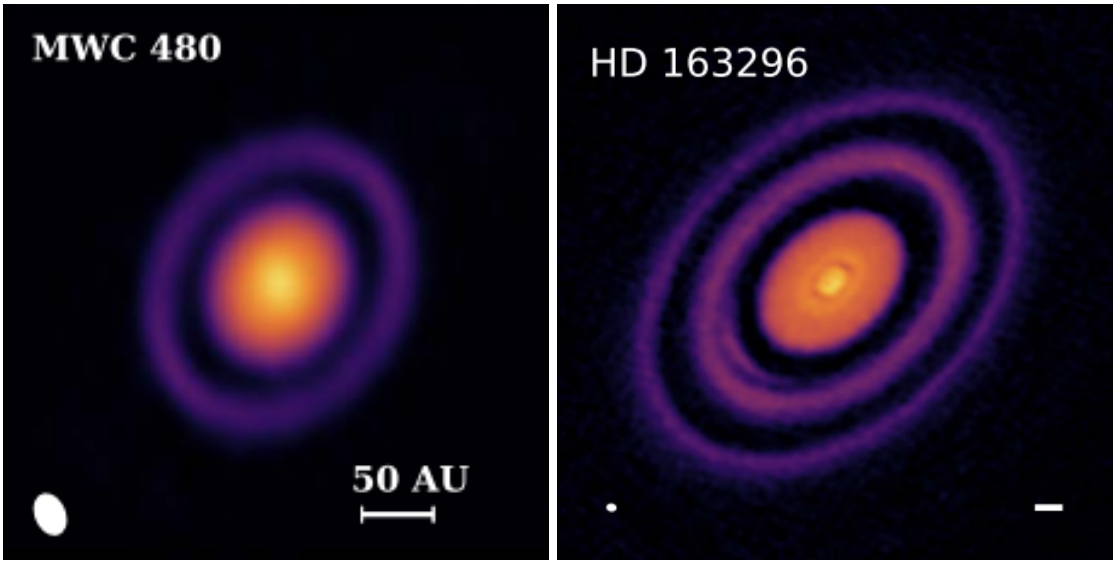

Figure 4: Disk structures of the protoplanetary disks studied in this thesis, beam size and image scale are shown in the bottom left and right corners of the panels respectively. The left panel shows MWC 480 by Long et al. (2018) in the 1.33 mm continuum. The right panel shows HD 163296 by Andrews et al. (2018) in the 1.25 mm continuum, with an image scale of 10 au.

methods to derive C/O ratios include using the column densities of sulfur molecules. As by Ma et al. (2024), who use the column density ratio of CS to SO to speculate that the C/O ratio in HD 163296 needs to be at least 1.1. Furthermore, many of these recent studies find that a C/O ratio that changes with radius from the star fits the derived column densities better than a constant C/O value throughout the disk. Importanly, the column densities used to derive the C/O ratios are never direct observations. Rather, intensity profiles are observed and computational models applied to those to derive column densities.

1.2 Observations

1.2.1 Interferometry

The observations used for this thesis are collected by the Atacama Large (sub)Millimeter Array (ALMA), which operates as an interferometer with its 66 telescope dishes (ALMA, 2021). Hence, I shall briefly describe the basics of interferometry.

An interferometer is a grouping of smaller, linked telescopes, allowing for a smaller angular resolution to be observed than a single dish would ever allow (Ilee and Greaves, 2015). The resolution of an interferometer is given by:

$$\text{Resolution} = \frac{\lambda}{2\text{b}} \tag{1}$$

where b is the baseline or the separation between the dishes (Monnier, 2003). So by increasing the distance between the telescopes linked in an interferometer, we can increase this baseline and thus observe a smaller angular resolution. By increasing the number of telescopes in the interferometer, we increase the sensitivity, total collecting area and number of baselines. This allows for the observation plane to be mapped out more completely. Since the observation plane needs to be inverted to form an image, a more complete plane will create a better image.

Of course, data cannot be collected in the areas between the dishes, which means assumptions have to be made regarding, for example, the symmetry of the observed object, to fill in the missing

areas in the image. Additionaly, due to Earth's natural rotation the collected observations form arcs. So a longer observation time, will produce a longer arc and thus, again, a more complete observation plane that is then inverted to form the images (Ilee and Greaves, 2015).

1.2.2 MAPS

The "Molecules with ALMA at Planet-forming Scales" or MAPS program is a recent collaboration that studied the chemistry in protoplanetary disks down to scales of 10 au (Öberg et al., 2021). Öberg et al. (2021) provide an overview of the program goals, introduce all the molecules, the lines that are studied and which bands they are observed in. Furthermore, they introduce the five disks studied in the MAPS program (IM Lup, GM Aur, As 209, HD 163296 and MWC 480) and explains why these were chosen as targets. As mentioned previously, in this thesis I will focus on the last two of those disks, since they are massive Herbig Ae disks with clear detections of both C_2H and C_3H_2.

Of the 20 molecules observed in the MAPS program, I will focus on C_2H and cyclic-C_3H_2, which I will refer to as simply C_3H_2. C_2H was chosen as it has been used in the MAPS program, by Bosman et al. (2021) in particular, to derive the C/O ratios in the protoplanetary disks. C_3H_2 was chosen because it is one of the largest molecules observed by the MAPS program. As a hydrocarbon, it can help to understand whether or not the chemistry in the protoplanetary disk is carbon based as expected from the enhanced C/O values. To understand the pathways that form and destroy these molecules in the disks I refer the reader to Kanwar et al. (2024) for both molecules.

1.3 This Thesis

Using the MAPS observations and ProDiMo models I will evaluate the necessity of enhanced C/O ratios in the two disks, and thus address to which extent processes, like the vertical cold finger effect, are necessary to explain the observations of these two protoplanetary disks.

By using two C/O ratios, one solar value of 0.46 and one enhanced value of 1.1, in the ProDiMo models for each of the two disks, four models will be obtained. These can then be compared to the MAPS observations, more specifically the integrated line fluxes, radial intensity profiles and the column density profiles derived in the MAPS analysis. The integrated line fluxes and radial intensity profiles provide a good measure of the overall strength of the molecular line emission and where the molecules are located in the disks respectively. Since the column densities are often used to derive the C/O ratios in disks, despite being derived values themselves, comparing the MAPS to the ProDiMo values can help provide insight into the setup and processes in the MAPS and ProDiMo models.

As will be described in Section 2, an important tool for these comparisons will be prodimopy to post-process the ProDiMo models and to obtain the molecular column densities. Another important tool will be GoFish (Teague, 2019). This is used in the MAPS papers to obtain the radial intensity profiles (Öberg et al., 2021) and so it will also be applied to the ProDiMo models to do the same. For the integrated line fluxes no processing was needed. Furthermore in Section 2, further details will be provided on the model analysis methods, details on the chosen molecular lines, the specifics of their observations and the calculation of radial intensity profiles. In Section 3, the results of the ProDiMo models will be presented and they will be compared to the MAPS observations. Finally in Section 4, the conclusions of this thesis will be presented.

2 Methods

2.1 Observations

The two molecules at the focus of this thesis are C_2H and C_3H_2, but as an extra check on the validity of the ProDiMo models CO is also included, as it is often used as a measure of the disk mass. The C_2H data is taken from Guzmán et al. (2021), the C_3H_2 data is from Ilee et al. (2021) and the CO data is from Zhang et al. (2021), all as a part of the MAPS project.

2.1.1 Observational Data

- Molecular Lines

Each of the molecules this thesis will focus on, has multiple possible lines that can be observed. A full overview of these is given by Öberg et al. (2021), but a condensed version is given below in Table 1. ALMA observations were done in either band 3 or band 6 and Table 1 lists which beam sizes were used in the observations.

Molecule	Quantum Numbers	ν_0 [GHz]	E_u [K]	A_{ij} [s^{-1}]	Beam [arcsec]
C_2H	N = 1-0, J = $\frac{3}{2}$-$\frac{1}{2}$, F = 2-1	87.316898	4.2	2.208×10^{-6}	0.3
C_3H_2	$(J_{K_a,K_b}) = 7_{07}$-6_{16}	251.314367	50.7	8.504×10^{-4}	0.15
CO	J = 2-1	230.538000	16.6	6.910×10^{-7}	0.15

Table 1: Overview of the molecular lines used in this thesis, ν_0 refers to the rest frequency, E_u to the excitation temperature of the upper molecular level and A_{ij} to the Einstein A coefficient

For CO, the line provided is the only one the MAPS team observed, although they did also look at other isotopologue lines. For C_2H and C_3H_2, on the other hand, multiple molecular lines were observed by the MAPS team. The ones chosen in Table 1 have the highest signal to noise ratio and thus should provide the clearest, most precise observations.

- Integrated Line Fluxes

The observations of the protoplanetary disks are collected as three dimensional data cubes, which is also what is produced by ProDiMo as output. In these cubes, the first two axes provide the position in the disk and the third axis the velocity. In order for the MAPS team to go from these cubes to the single value of the integrated line flux some computational processing is required. This processing is done with, for example, the GoFish package (Teague, 2019), which uses the velocity axis to consider the rotation of the disk and collapse the cube into two dimensional data output. As described by Ilee et al. (2021), the GoFish package and its integrated_spectrum function can be used for this. This function provides the flux as a function of velocity in the disk. By then integrating over the velocity, the integrated line flux is derived in units of [Jy km/s].

- Radial Intensity Profiles

Law et al. (2021) describes how the radial intensity profiles were obtained for all the molecular lines observed in the MAPS program. Before the intensity profiles can be generated, maps of the velocity-integrated intensity, so-called moment-0 maps, need to be created. Examples of these moment-0 maps for the CO 2-1 line can be seen in Figure 5. These maps can then be used as input in the radial_profile function of GoFish to obtain the radial intensity profiles in [Jy/beam km/s], or some other unit of this quantity.

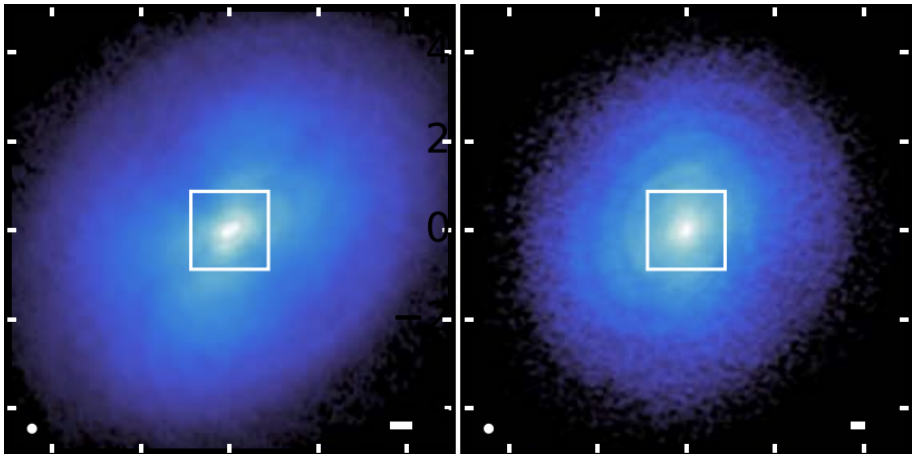

Figure 5: Moment-0 maps of CO 2-1 in HD 163296 (left) and MWC 480 (right), the synthesised beam and scale bar for 50 au are in the lower left and right corners respectively. The white rectangle indicated the field of view of the continuum images (not shown here). The axes are the angular offset from the center with each tick representing 2" (Law et al., 2021)

- Column Densities

As mentioned in Section 1.1.8, the column densities of the MAPS project are derived using models. By assuming local thermal equilibrium (LTE) for the emission, and given the fact that ALMA has observed multiple lines of the molecules, the column density can be derived as

$$N_u = \frac{N_{tot}}{Q(T_{ex})} \cdot g_u \cdot \exp\left(\frac{-E_u}{k \cdot T_{ex}}\right) \tag{2}$$

Where N_{tot} is the total column density, N_u is the upper-level column density, g_u is the upper-level degeneracy, E_u is the upper-level energy, $Q(T_{ex})$ is the partition function, T_{ex} is the excitation temperature and k is the Boltzman constant. A full derivation of this is given by Ilee et al. (2021). Markov Chain Monte Carlo modelling was then used to achieve the best fit values of the total column density. Because of the modeling step required to obtain the column densities, this would not be a good parameter to check the validity of the ProDiMo model. However, comparing the MAPS to the ProDiMo hydrocarbon column densities can help explain where any potential difference in C/O conclusion originates from. Unfortunately, Zhang et al. (2021) does not provide CO column densities so the column density comparison will be limited to C_2H and C_3H_2.

2.2 ProDiMo

2.2.1 Disk Models

The ProDiMo models were calculated using two different C/O values for MWC 480 and HD 163296. The most important input parameters are listed in Table 2 for the stellar properties and Table 3 for the disk properties. A more extensive list of input values can be found in Woitke et al. (2019), where many objects in the DIANA project were carefully fitted to observations. In Table 3, there are radii and masses shown for two zones within both the MWC 480 and HD 163296 disks. Most notably, there is a gap between these inner and outer zones that can be expected to also show up in any data extracted from the model.

Besides all these input parameters, elemental abundances are also be entered into the models. The C/O ratio has two values for each disk, creating a total of four models. The C/O values used

Disk	distance [pc]	inclination [deg]	$M_\star$ [$M_\odot$]	$L_\star$ [$L_\odot$]	$T_{\rm eff}$ [K]
MWC 480	156.2	37.5	2.05	17.809	8250
HD 163296	101	50	2.0	25.165	9000

Table 2: Stellar input parameters for the ProDiMo models

Disk	$r_{\rm in}$ [au]	$r_{\rm out}$ [au]	m [$M_\odot$]	$R_{\rm in}$ [au]	$R_{\rm out}$ [au]	M [$M_\odot$]
MWC 480	0.256	4.61	1.32×10^{-6}	49.3	829.2	0.0442
HD 163296	0.446	10.05	2.12×10^{-4}	24.0	780.3	0.0512

Table 3: Disk input parameters for the ProDiMo models, r and m are used for the size and mass of the inner disk zone, and R and M for the outer disk zone

are 0.46, the solar C/O ratio, and 1.1, as an enhanced C/O value. Which is not as high as the extreme values suggested by Alarcón et al. (2021) or Bosman et al. (2021), rather it is based on chemistry as described by, for example, Najita et al. (2011). They explain how once CO forms, carbon is left in the disk instead of oxygen. This allows for additional carbon chemistry and since there is still a lot of hydrogen but no longer much oxygen, hydrocarbons are the preferred product formed. To achieve the enhanced C/O ratio, the oxygen abundance is depleted in the disk models.

2.2.2 Extracting Observables

With the models in hand, we can start extracting the data that we need to match the aforementioned observables from the MAPS project.

- Integrated Line Fluxes

The integrated line fluxes are given as direct output by the ProDiMo code, although in units of W/m^2. Since the MAPS line fluxes are given in Jy km/s, the following unit conversion has been applied:

$$\frac{F}{\mathrm{Jy\,km/s}} = c \cdot 10^{17} \left(\frac{\nu_0}{\mathrm{GHz}}\right)^{-1} \left(\frac{F}{W m^{-2}}\right) \tag{3}$$

whereere F is the line flux, c is the speed of light in km/s and ν_0 is the line frequency.

- Radial Intensity Profiles

Before extracting the radial intensity profiles the data cubes of the ProDiMo models have to be convolved to account for the beam size used in the observations. The spectral_cube and radio_beam packages are used to do this. The functions needed are Spectralcube.read() to read the original data cube and Spectralcube.with_beam() to input the pixel size of the unconvolved cube as the initial beam size. Finally, the Spectralcube.convolve_to () function is used to convolve the cube to the beam we want, 0.3 arcsec for C_2H and 0.15 arcsec for CO and C_3H_2. To input these beams, the radio_beam.Beam() function is used. This creates a fits file with the newly convolved data cube. The header of the unconvolved cube is copied to the newly convolved cube, as it is needed in the GoFish input, with added parameters for the beam major and minor axes and the beam position angle. The additional values used in these headers are listed in Table 4. The beam sizes in the header are larger than used in the convolution for CO and C_3H_2. This is to ensure GoFish can read the cubes, as with a smaller beam an error occurs when it calculates the pixel sizes.

Molecule	MWC 480			HD 163296		
	BMIN [deg]	BMAJ [deg]	BPA [deg]	BMIN [deg]	BMAJ [deg]	BPA [deg]
C_2H	8.33×10^{-05}	8.33×10^{-05}	148	8.33×10^{-05}	8.33×10^{-05}	133.3
C_3H_2	4.86×10^{-05}	4.86×10^{-05}	148	5.75×10^{-5}	5.75×10^{-5}	133.3
CO	4.86×10^{-05}	4.86×10^{-05}	148	5.75×10^{-5}	5.75×10^{-5}	133.3

Table 4: Beam variables added to the headers of the convolved ProDiMo data cubes

With the fits files of the convolved data cubes, the same radial_profile function in GoFish that was used in the MAPS papers is applied to the ProDiMo data cubes. The entire cube is given as input to GoFish, after which the function calculates the moment-0 map and with it the radial intensity profile.

In the MAPS papers, the radial intensity profiles are given in units of [Jy/beam m/s]. To be able to quantitatively compare the MAPS and ProDiMo radial intensity profiles, the webplotdigitizer tool by Rohatgi (2024) is used. This creates a data file with the values from the MAPS papers that can then be used to compare to the ProDiMo observables.

- Column Densities

To extract the column densities from the ProDiMo models the plot_cdnmol function in prodimopy is used. This function reads in the ProDiMo model and returns the vertical column densities of the molecules given as input in the function. The function produces column densities in units of cm^{-2}, which is the same as the column densities in the MAPS papers. In order to quantitatively compare the two, the webplotdigitizer tool is used again.

3 Results and Discussion

3.1 Integrated Line Fluxes

A first check on the validity of the models is to look at the integrated line fluxes, listed in Table 5. In the solar C/O models, the difference between the ProDiMo models and MAPS observations are a factor 2.4 and 0.36 for the C_2H for MWC 480 and HD 163296 respectively, for C_3H_2 the respective differences are 2.9 and 2.0. In the enhanced C/O models, for MWC 480 and HD 163296 respectively the differences in the C_2H integrated line flux are factors 10.5 and 4.2 and for C_3H_2 those numbers are 38.1 and 35.4. From this comparison it is clear that the disk models with the solar C/O value matches the observations better.

For CO, the difference between all four ProDiMo models and MAPS observations is consistently around a factor 1.6. Indicating that the CO flux is largely independent of the C/O ratio as it does not change significantly between the solar and enhanced C/O models. Despite CO being one of the main carriers of oxygen in protoplanetary disks. Based on that, it could be expected that depleting the disk of oxygen, would lead to a lower CO flux, but this is evidently not the case.

It is interesting, however, that all ProDiMo fluxes are usually larger than the MAPS values, the sole exception being the C_2H integated line flux in the solar C/O HD 163296 model. Hence, this is investigated further by studying the line emitting regions and the two dimensional abundance maps.

Molecule	Integrated Line Fluxes [Jy km/s]					
	MWC 480			HD 163296		
	MAPS	C/O = 0.46	C/O = 1.1	MAPS	C/O = 0.46	C/O = 1.1
C_2H[1]	0.0443 ± 0.0172	0.1051	0.4643	0.1301 ± 0.0342	0.04648	0.5479
C_3H_2[2]	0.1199 ± 0.0032	0.3499	4.573	0.1468 ± 0.0028	0.296	5.192
CO[3]	23.226 ± 0.063	36.93	37.96	45.246 ± 0.102	73.12	74.96

Table 5: Integrated line fluxes in the ProDiMo models and MAPS observations

With the integrated line fluxes, it is important to keep in mind that the line emission scales with the emitting surface area. Therefore, they contain no spatial or spectral information and we need to consider, for example, the radial intensity profiles for this.

Figure 6 shows the two dimensional gas abundance of each of the molecules. On top of that, it also shows the main emitting region of the molecular lines mentioned in Table 1. From these, it is clear that in each of the models, the line fluxes originate in the outer disk, well beyond the gaps. Hence, why only the gas beyond the gap is shown in the plots. Particularly for C_2H and C_3H_2 in the solar C/O models, the line origin is close to the outer edge, where the molecular abundances taper off. For these molecules in the enhanced C/O models, the emitting areas are more widespread, offering an explanation for the increase in integrated line flux in these models. However, for optically thick lines extending the emitting area inwards into the disk does not increase the emitting surface area and thus does not affect the integrated line flux. For these, an

[1]MAPS C_2H integrated line fluxes from (Guzmán et al., 2021)
[2]MAPS C_3H_2 integrated line fluxes from (Ilee et al., 2021)
[3]MAPS CO integrated line fluxes from (Öberg et al., 2021)

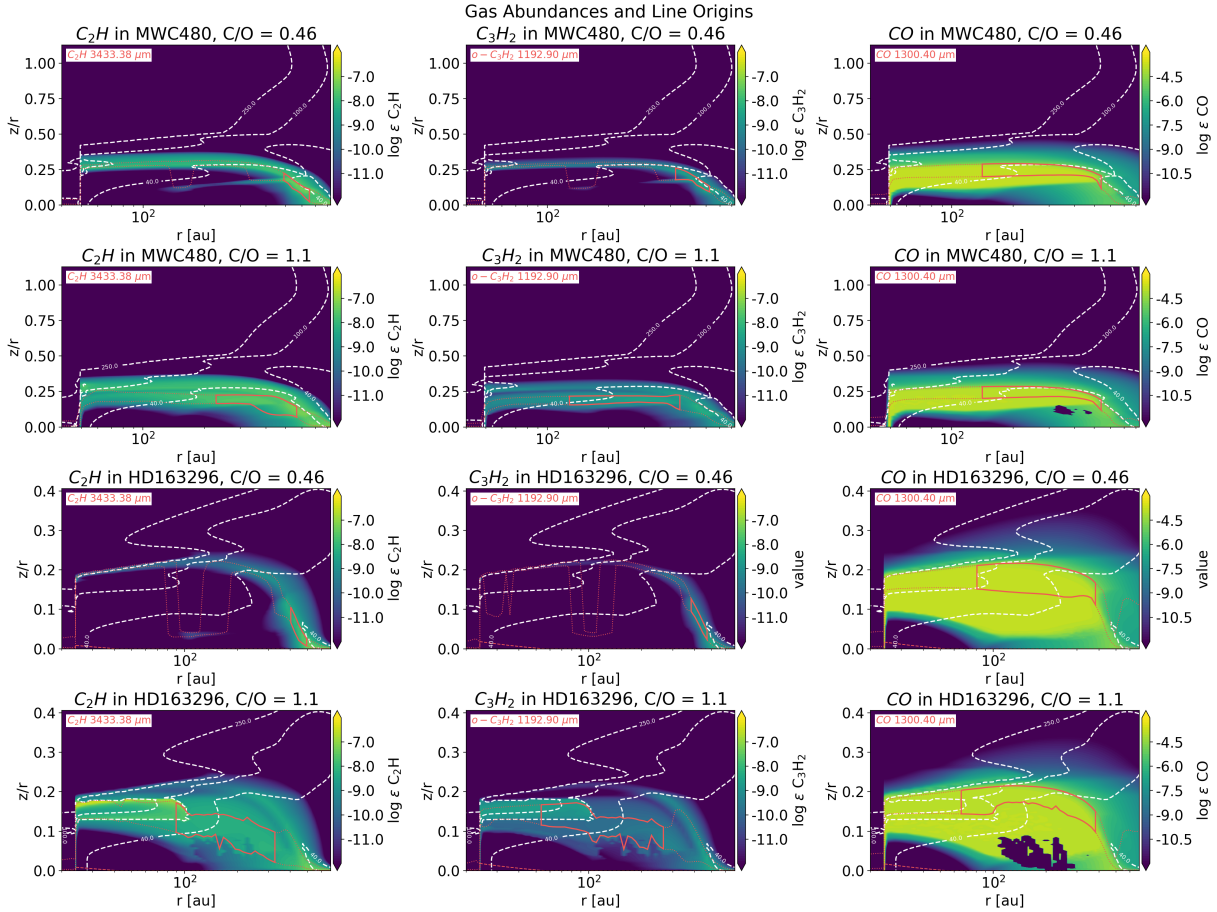

Figure 6: Gas Abundances and line emitting regions (indicated by the red boxes) of C_2H, C_3H_2 and CO in the outer regions of all 4 ProDiMo models. Temperature contours at 250, 100 and 40K are marked in white. The colourbars show the abundance of the molecules (log values).

alternative explanation for an increased line flux may be found by investigating the average gas temperatures in the line emitting regions.

The large increase in the abundances of C_2H and C_3H_2 from the solar to the enhanced C/O models can be explained by the low temperatures in these regions. This causes water, the main carrier of oxygen, to freeze out. Meaning that all the oxygen is now bound to the surface of dust grains, while the carbon remains free to participate in the gas chemistry. This lower abundance of oxygen forces the carbon to mainly react with hydrogen to form hydrocarbons, causing the increased abundances seen in Figure 6.

From the average gas temperatures shown in Table 6, the integrated line fluxes are further explained. The large increase in the C_3H_2 integrated line flux from the solar to the enhanced C/O models in both disks is reflected in the large increase in temperature of the corresponding line emitting region. For C_2H in HD 163296 a similarly large increase in both gas temperature and integrated line flux is seen, while for C_2H in MWC 480 a minor increase in gas temperature also leads to a minor increase in the integrated line flux. From the gas temperatures in HD 163296, it becomes clear that despite the oxygen and CO depletion in the enhanced C/O model, the increase in temperature compensates for this and produces a similar integrated line flux to the solar C/O model. Interestingly, there is no such increase in MWC 480, the temperature actually decreases slightly, and the CO emitting regions in the two models are also very similar as seen

in Figure 6. So more research is needed to provide an explanation behind the approximately constant CO integrated line fluxes in the MWC 480 models.

Molecule	Average gas temperatures [K]			
	MWC 480		HD 163296	
	C/O = 0.46	C/O = 1.1	C/O = 0.46	C/O = 1.1
C_2H	21.25	22.35	20.05	38.15
C_3H_2	25.46	32.59	23.25	55.55
CO	35.24	32.86	59.51	89.83

Table 6: Average gas temperatures in the line emitting regions, weighted with gas mass

These gas temperatures also explain the difference in the integrated line fluxes of C_2H and C_3H_2. Looking at the abundance maps, C_2H consistently has a higher abundance in the outer disks compared to C_3H_2, while its integrated line flux is lower. From Table 6 we see that C_3H_2 has considerably higher average gas temperatures, especially for the enhanced C/O models. This higher gas temperature explains why, despite lower abundances, C_3H_2 has higher integrated line fluxes than C_2H.

The CO abundance maps in Figure 6 show voids in the outer regions of the enhanced C/O disk models. These are due to the non-convergence of chemistry in these regions of the models. This means that the ProDiMo model is unable to solve the CO chemistry in these regions, causing a void to appear in the abundance maps.

To further confirm whether or not the chemistry in disks is truly carbon rich, as should be the case when there is an enhanced C/O ratio, more large carbon molecules should be observed. If longer carbon chains can be found in the outer regions of protoplanetary disks, this would be more conclusive evidence that the chemistry there is, in fact, carbon rich. This could be tested in the ProDiMo models by looking at the abundances of molecules with longer carbon chains. If the enhanced C/O model were to show a significant increase in the abundance of longer carbon molecules, that would indicate a more carbon rich chemistry.

3.2 Radial Intensity Profiles

As a next step, we compare the radial intensity profiles (Figure 7). The models and observations generally follow the same shape, specifically that the peak intensity is around the same radius within the disk. However, there are large differences in the values of these peak intensities.

What is interesting with these peak intensities is that for C_2H and CO the peak intensities are lower in the ProDiMo models than the MAPS observations, while for C_3H_2 the opposite is true. For C_3H_2 and CO the beam size used by GoFish to calculate the profiles is slightly off from the ALMA beams used in the MAPS observations, but this difference in beam sizes is not big enough to account for the difference in the peak intensities of the line profiles. Especially considering that the ProDiMo models have been convolved with the correct beam sizes. For future research, it could be prudent, however, to also perform convolutions using other software, like the CASA package, to check the validity of the current convolution method.

While the C_2H integrated line fluxes were reasonably similar between the models and the observations, the intensity profiles show a severe lack in C_2H flux. The slight peaks in the model profiles are, at least, at similar radii as the peak in the model profiles, but there is just over an order of magnitude difference between the intensity values. In the HD 163296 MAPS observations there are two clear peaks in the C_2H intensity, indicating two gaps in the disk, while only one can be seen in the ProDiMo models. This is likely because the ProDiMo model is set

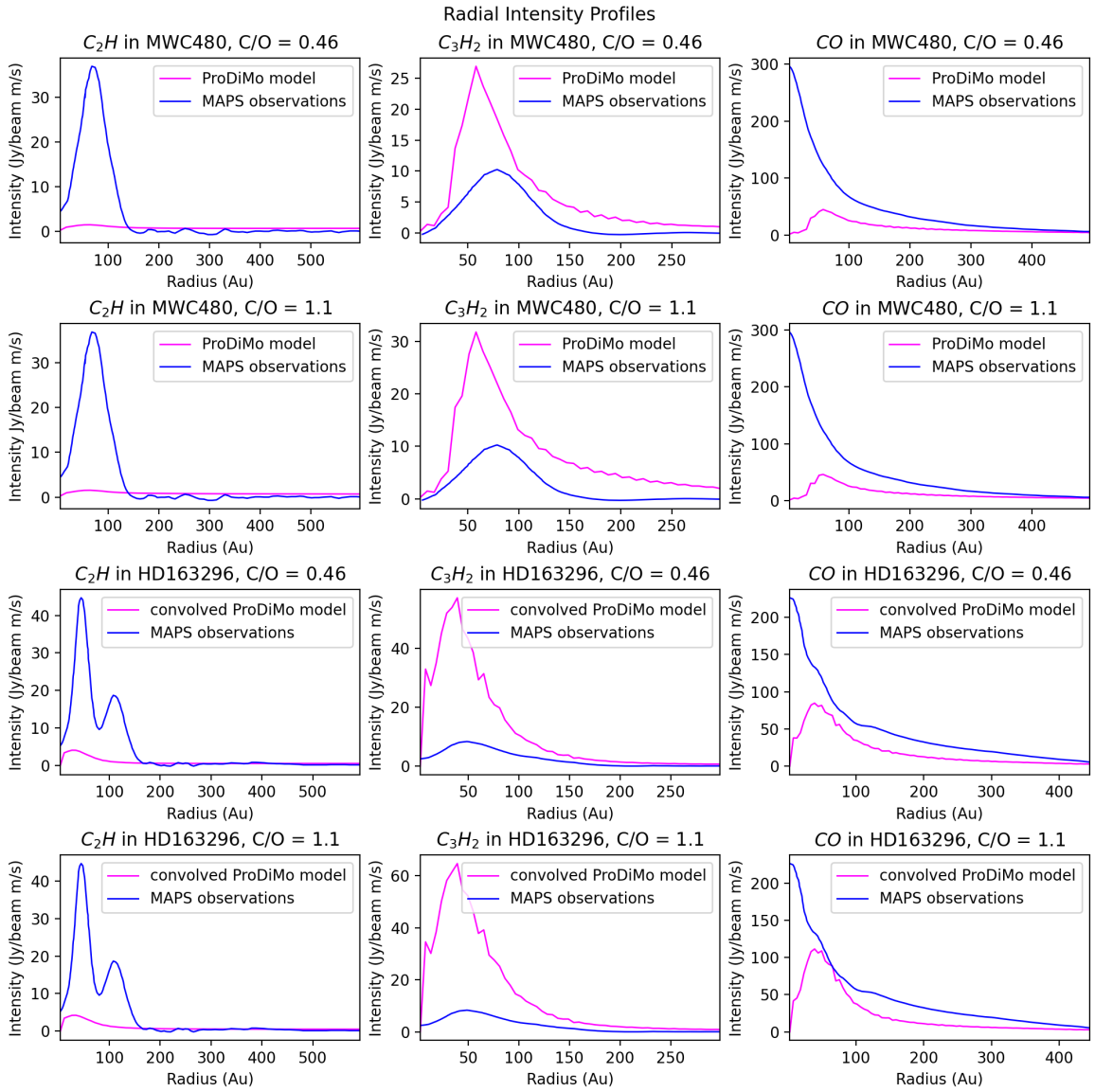

Figure 7: Convolved radial intensity profiles for the ProDiMo models (in pink) and the MAPS observations (in blue). The plots only go out to the furthest radii of the MAPS intensity profiles

up to have two zones, instead of the three that are indicated by the observations, which could be considered as an improvement in future models. Beyond these peaks, in the outer regions of the disk (beyond 200 au) the models and observations do show very similar, albeit low, values.

In the MWC 480 models, the difference between the ProDiMo models and the MAPS observations of C_3H_2 is only about a factor 3. But in the HD 163296 models this factor doubles, with the models indicating that HD 163296 has about double the C_3H_2 flux from MWC 480 while the MAPS observations suggest similar fluxes from the disks. Once again, towards the outer disks, the profiles at least tend towards similarly low values, especially for HD 163296 the C_3H_2 profiles come together nicely further out in the disk.

For CO, the MAPS observations measure significantly more flux towards the very centre of the disk, which is missing in the ProDiMo models. However, at the position of the ProDiMo peak intensity in the HD 163296 models, there seems to be a slight change in slope of the MAPS intensity profile. After this peak in the ProDiMo models, the MAPS and ProDiMo profiles

largely follow the same trajectory in the outer regions of the disk. For the MWC 480 models, the profiles are also decently similar in the outer regions of the disk.

From the abundance maps of C_2H and C_3H_2 in Figure 6 we see lower abundances of C_3H_2. From those alone, we might have expected the C_3H_2 intensity profiles to be lower as well, but the profiles in Figure 7 tell a different story. There we see significantly higher peak intensities for C_3H_2 than C_2H. An explanation for this might be found in the Einstein A coefficients of the molecules. These relate to the probability of spontaneous emission of a particular molecular transition (Hilborn, 2002) and are shown in Table 1. As explained by Guzmán et al. (2021), the line intensity is calculated using the following equation:

$$I_\nu = [B_\nu(T_{ex}) - B_\nu(T_{bg})] \cdot [1 - \exp(-\tau_\nu)] \tag{4}$$

where B_ν is the Planck function, T_{ex} is the excitation temperature, T_{bg} is the background temperature and τ_ν is the optical depth of the line. This line optical depth is calculated as follows:

$$\tau_\nu = \frac{A_{ul} \cdot c^3 \cdot N_u}{8\pi \cdot \nu^3 \cdot \sigma \cdot \sqrt{2\pi}} \left[\exp\left(\frac{h \cdot \nu}{k \cdot T_{ex}}\right) - 1\right] \tag{5}$$

where A_{ul} is the Einstein A coefficient, N_u is the upper level column density, ν is the line frequency and σ is the Gaussian line width. From these equations it becomes clear that the intensity of a line depends on the frequency, excitation temperature, column density and Einstein A coefficient of the line. Furthermore, an optically thick line will also have a higher line intensity than an optically thin line. From the Einstein A coefficients in Table 1, it is clear that it is significantly more likely for the C_3H_2 transition to occur than for the C_2H transition. Furthermore from Table 1, we see that the rest frequency and excitation temperature of C_3H_2 are also higher than those of C_2H. All of this combines to ensure that the transition which is more likely to occur will produce a higher intensity flux than the transition which is less likely to occur. Thus we see a higher peak intensity for C_3H_2 than for C_2H.

To account for the missing C_2H intensity in the future, more gas could be added to the inner 100 to 200 au of the disk. Especially since changing the C/O ratio of the disk is not enough to provide the missing flux. If adding additional gas in the ProDiMo models does not work, the chemical network or outer disk structure could potentially be revised to allow the creation of more C_2H and less C_3H_2 to more closely reproduce the MAPS observations.

Since the MAPS observations generally stop at a significantly smaller radius than the ProDiMo models, the plots in Figure 7 have been limited to only show the radii where there is MAPS and ProDiMo data. As described by Law et al. (2021), the MAPS radii are constrained to the radius that contains 90% of the flux. In their paper, they mention that emission is often also observed beyond these radii, but that this is "diffuse, low flux emission". In both the solar and enhanced C/O ProDiMo models, on the other hand, the entire disk radius is also assumed to be the gas disk radius for each of the molecules. So the ProDiMo data not take into account a constraint on the flux. The respective gas disk radii can be found in Table 7. Furthermore, the abundance maps in Figure 6 suggest considerable abundances of the molecules beyond the 90% flux radius in the MAPS data. This could indicate that the ProDiMo models taper off slower than the disks in the MAPS observations and that this should be taken into account in future research. On the other hand, the ProDiMo intensity profiles fall towards 0 before reaching the outer radii of the MAPS observations. Which indicates that the molecular abundances in the outermost regions of the ProDiMo disks does not contribute significantly to the intensity profile and the outer radii of the models and observations do not significantly affect our results.

Since all three molecules have decent agreement in the radial intensity profiles between the MAPS observations and ProDiMo models in the outer regions of the disks when there are still

Disk	Outer Gas Disk Radii [au]			
	100% flux	90% flux		
	ProDiMo	C_2H MAPS	C_3H_2 MAPS	CO MAPS
MWC 480	829.17	103 ± 13	113 ± 12	309 ± 6
HD 163296	780.29	144 ± 56	136 ± 13	308 ± 4

Table 7: Outer gas disk radii in the ProDiMo models containing all the flux and the disk radii containing 90% of the flux in the MAPS observations taken from Law et al. (2021).

observations, the ProDiMo models seems to be the most valid there. Meaning that the models could potentially be a very useful way to qualitatively study the chemistry in the outermost regions of the disk. Especially when considering the flux levels are often too low to measure so far out.

Overall, the differences between the solar and enhanced C/O ProDiMo models in the radial intensity profiles are not significant enough to allow for a definitive conclusion regarding the accuracy of one over the other. While the peak intensities do go up from the solar to the enhanced C/O models, the change is not large enough to create a clear preference for either of the models. So, if anything, it can be said that choosing the C/O ratio of a protoplanetary disk cannot be decided on the radial intensity profiles, or at least not these profiles alone.

3.3 Column Densities

Contrary to the integrated line fluxes or radial intensity profiles, the vertical column densities of the molecules in the enhanced C/O models, as seen in Figure 8, agree better with those derived by the MAPS team. For both molecules, the solar C/O models have column densities that are about two orders of magnitude smaller than those derived by the MAPS team from the observations. Meanwhile, the magnitudes of the enhanced C/O models' column densities are similar to those from the MAPS papers.

In MWC 480 for both C_2H and C_3H_2, the magnitudes of the enhanced C/O model column densities and the MAPS column densities are similar, while the solar C/O model column densities are about 2 orders of magnitude lower. In HD 163296, the solar C/O models are also about two orders of magnitude lower than the column densities derived by the MAPS team, while the enhanced C/O models have similar magnitudes. This suggests that the enhanced C/O models more accurately reproduce the model used by the MAPS team to derive column densities.

While the magnitudes of the column densities show decent agreement between the ProDiMo model and MAPS observations, the shapes of the plots are not similar in most of the graphs. Only the enhanced C/O model for HD 163296 has a column density plot that has at least somewhat of a similar shape. It should be kept in mind that the observations go out to a smaller radius than the models because of the smaller gas disk radii as described in Table 7. However, since 90% of the observed flux is included within those gas disk radii, the column densities beyond them likely will not be as significant as in the models. This could indicate, once again, that the ProDiMo disk model should taper off more quickly than they currently do. At least to more closely reproduce the MAPS results. The enhanced C/O disk models do show decreasing column densities towards the outer radius, similar to the MAPS column densities, but the models still decrease less rapidly, which could be resolved with a steeper tapering off in the ProDiMo models.

A further interesting point is that the ProDiMo models show a clear gap in the column densities of C_2H and C_3H_2, located at the same position as the dust gap. Law et al. (2021) does confirm substructures of C_2H and C_3H_2 around the radius of this dust gap, but the column densities derived by Ilee et al. (2021) and Guzmán et al. (2021) do not reflect this. This suggests

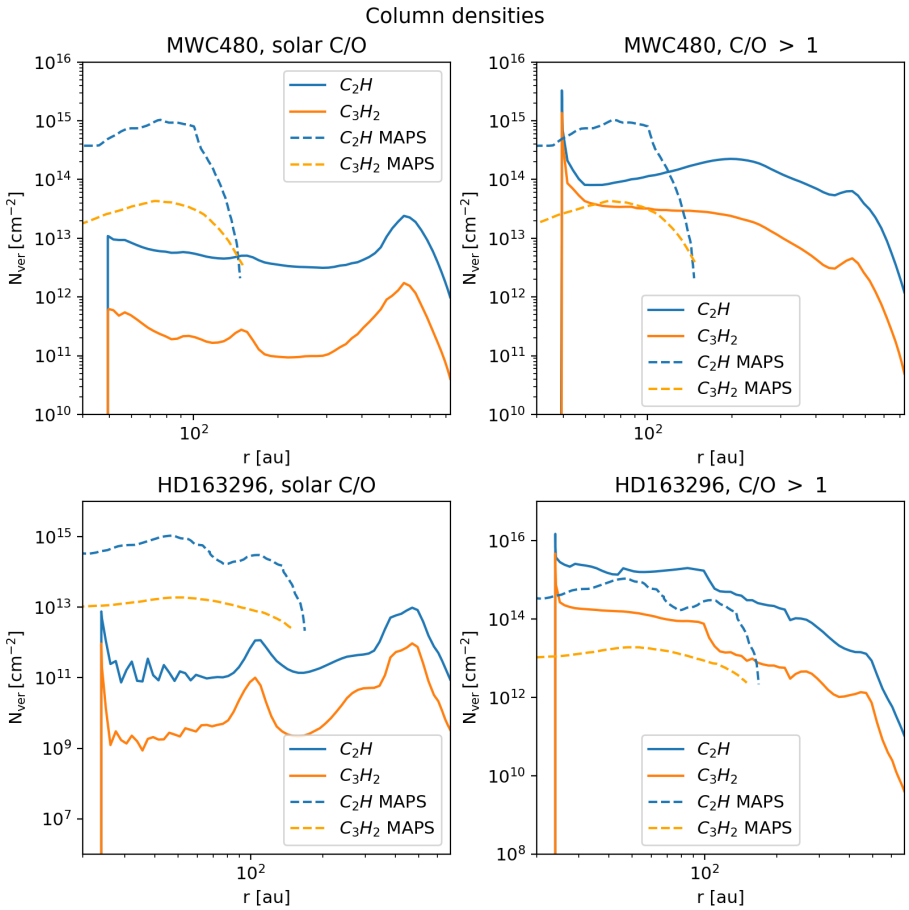

Figure 8: Vertical column densities for C_2H (solid blue) and C_3H_2 (solid orange) in the ProDiMo models and C_2H (dashed blue) and C_3H_2 (dashed orange) in the MAPS observations. The plots are focused on the disk beyond the gap

that a gap in the dust does not equate to a gap in the gas, something that should be taken into account in future reruns of the ProDiMo models.

Since the column densities are not observables but rather derived values, it should be considered that the models used by the MAPS team introduce a level of uncertainty into the results and hence, cannot be taken at face value. Furthermore, the MAPS team uses time dependent chemistry in their models, like in Bosman et al. (2021), while ProDiMo uses steady state chemistry. This indicates that when comparing protoplanetary disk models and observations, the column density of a molecule is not a suitable variable for determining the C/O ratio in the disk.

What can be derived from comparing the column densities from the ProDiMo models and the MAPS derivations is some of the underlying structure of the models. For the enhanced C/O ProDiMo models in particular, the C_2H column densities approach or even exceed the MAPS values, while from Figure 7, we recall that the intensity profile is significantly lower than the MAPS observations. This suggests that the models used by the MAPS team require higher column densities than the ProDiMo models to obtain the same intensities. Which indicates that ProDiMo produces more emission and could hint at higher temperatures or larger emitting regions in the ProDiMo models compared to the MAPS models.

4 Conclusion

The most important conclusion from the results is that the C/O ratio in MWC 480 and HD 163296 is not as high as the value of 2 suggested by Bosman et al. (2021). This is based on the integrated line fluxes of thermo-chemical disk models, where the solar C/O ratio produced values most similar to the observed MAPS integrated line fluxes. From the radial intensity profiles, no clear conclusion could be drawn on what the C/O value should be in the disks as it was found that enhancing the C/O ratio does not significantly alter the intensity flux. Since the column densities are not observables, but rather derived from models, whether that be ProDiMo or the model used by the MAPS team, they should not be used to definitively determine the C/O ratio in a protoplanetary disk.

Looking back at the MAPS project, Bosman et al. (2021) concluded that to explain the C_2H column densities, a C/O ratio of 2 was needed. The ProDiMo models, however, are able to derive similar column densities at a C/O ratio of 1.1, pointing to differences in the models used to obtain the column densities, like higher gas temperatures or larger emitting regions. Additionally, because the radial intensity profiles do not change significantly from the solar to the enhanced C/O ProDiMo model, this suggests that an enhanced C/O ratio might not be the solution to the high hydrocarbon intensities in protoplanetary disk observations.

Since the MAPS observations can be reproduced with significantly lower C/O ratios using ProDiMo, the results suggest that the need for processes like the cold finger effect might be overstated. The effect is still needed to create the oxygen depletion in the enhanced C/O ProDiMo models, but seems to not be as vital to protoplanetary disk chemistry as has been suggested.

To further narrow down the value of the C/O ratio in MWC 480 and HD 163296, more ProDiMo models can be run with varied C/O values between 0.46 and 1.10. Following the same methods as for the already existing models, a more exact conclusion on the C/O ratio in protoplanetary disks could be reached.

Furthermore, C/O ratios that are larger than 1, indicate a carbon rich chemistry. To confirm this, investigations can be done into larger carbon based molecules. If, for example, future ALMA observations can detect longer carbon chains in protoplanetary disks, their presence can then be taken into account more in models like ProDiMo to study the precise chemistry in more detail. Investigations into the abundances of the longer carbon molecules in ProDiMo with varying C/O ratios to see if a higher C/O leads to a significantly higher abundance. Thus this can provide more evidence for the claims that the chemistry in the outer regions of protoplanetary disks is largely carbon based.

Finally, the results showed that for the outermost regions of the disks, the MAPS observations could not provide data, because they were limited by the ALMA sensitivity. Hence they focused on the regions in which 90% of the flux was included, while the ProDiMo models have no such limitations. Deeper ALMA integrations in the future could help provide data on these outer regions, but in the mean time, ProDiMo models could be used to study the outer 200 to 300 au of protoplanetary disks. Especially considering that further out into the disk the radial intensity profiles of the ProDiMo models more closely resembled the MAPS observations. So while the ProDiMo models and the MAPS observations might not completely agree up to 400 or 500 au into the disk, for the regions where observations are not yet available, thermo-chemical models like ProDiMo are currently the best way to study the chemistry in these regions.

References

Alarcón, F., Bosman, A. D., Bergin, E. A., Zhang, K., Teague, R., Bae, J., Aikawa, Y., Andrews, S. M., Booth, A. S., Calahan, J. K., Cataldi, G., Czekala, I., Huang, J., Ilee, J. D., Law, C. J., Le Gal, R., Liu, Y., Long, F., Loomis, R. A., Ménard, F., Öberg, K. I., Schwarz, K. R., van't Hoff, M. L. R., Walsh, C., and Wilner, D. J. (2021). Molecules with ALMA at Planet-forming Scales (MAPS). VIII. CO Gap in AS 209-Gas Depletion or Chemical Processing? *ApJS*, 257(1):8.

ALMA (2021). Global Collaboration | ALMA — almaobservatory.org. https://www.almaobservatory.org/en/about-alma/global-collaboration/. [Accessed 02-07-2024].

Andrews, S. M. (2020). Observations of Protoplanetary Disk Structures. *ARAA*, 58:483–528.

Andrews, S. M., Huang, J., Pérez, L. M., Isella, A., Dullemond, C. P., Kurtovic, N. T., Guzmán, V. V., Carpenter, J. M., Wilner, D. J., Zhang, S., Zhu, Z., Birnstiel, T., Bai, X.-N., Benisty, M., Hughes, A. M., Öberg, K. I., and Ricci, L. (2018). The Disk Substructures at High Angular Resolution Project (DSHARP). I. Motivation, Sample, Calibration, and Overview. *ApJL*, 869(2):L41.

Bergin, E. A., Booth, R. A., Colmenares, M. J., and Ilee, J. D. (2024). C/O Ratios and the formation of wide separation exoplanets. *arXiv e-prints*, page arXiv:2406.12037.

Bosman, A. D., Alarcón, F., Bergin, E. A., Zhang, K., van't Hoff, M. L. R., Öberg, K. I., Guzmán, V. V., Walsh, C., Aikawa, Y., Andrews, S. M., Bergner, J. B., Booth, A. S., Cataldi, G., Cleeves, L. I., Czekala, I., Furuya, K., Huang, J., Ilee, J. D., Law, C. J., Le Gal, R., Liu, Y., Long, F., Loomis, R. A., Ménard, F., Nomura, H., Qi, C., Schwarz, K. R., Teague, R., Tsukagoshi, T., Yamato, Y., and Wilner, D. J. (2021). Molecules with ALMA at Planet-forming Scales (MAPS). VII. Substellar O/H and C/H and Superstellar C/O in Planet-feeding Gas. *ApJS*, 257(1):7.

Cleeves, L. I. (2018). Zooming in on the Chemistry of Protoplanetary Disks with ALMA. In Cunningham, M., Millar, T., and Aikawa, Y., editors, *Astrochemistry VII: Through the Cosmos from Galaxies to Planets*, volume 332, pages 57–68.

Dominik, C. (2015). Disk formation and structure. In *European Physical Journal Web of Conferences*, volume 102 of *European Physical Journal Web of Conferences*, page 00002.

Dong, R., Liu, S.-y., Eisner, J., Andrews, S., Fung, J., Zhu, Z., Chiang, E., Hashimoto, J., Liu, H. B., Casassus, S., Esposito, T., Hasegawa, Y., Muto, T., Pavlyuchenkov, Y., Wilner, D., Akiyama, E., Tamura, M., and Wisniewski, J. (2018). The Eccentric Cavity, Triple Rings, Two-armed Spirals, and Double Clumps of the MWC 758 Disk. *ApJ*, 860(2):124.

Guzmán, V. V., Bergner, J. B., Law, C. J., Öberg, K. I., Walsh, C., Cataldi, G., Aikawa, Y., Bergin, E. A., Czekala, I., Huang, J., Andrews, S. M., Loomis, R. A., Zhang, K., Le Gal, R., Alarcón, F., Ilee, J. D., Teague, R., Cleeves, L. I., Wilner, D. J., Long, F., Schwarz, K. R., Bosman, A. D., Pérez, L. M., Ménard, F., and Liu, Y. (2021). Molecules with ALMA at Planet-forming Scales (MAPS). VI. Distribution of the Small Organics HCN, C_2H, and H_2CO. *ApJS*, 257(1):6.

Helled, R., Bodenheimer, P., Podolak, M., Boley, A., Meru, F., Nayakshin, S., Fortney, J. J., Mayer, L., Alibert, Y., and Boss, A. P. (2014). Giant Planet Formation, Evolution, and

Internal Structure. In Beuther, H., Klessen, R. S., Dullemond, C. P., and Henning, T., editors, *Protostars and Planets VI*, pages 643–665.

Herbig, G. H. (1960). The Spectra of Be- and Ae-Type Stars Associated with Nebulosity. *ApJS*, 4:337.

Hilborn, R. C. (2002). Einstein coefficients, cross sections, f values, dipole moments, and all that. *arXiv e-prints*, page physics/0202029.

Ilee, J. D. and Greaves, J. S. (2015). Interferometry and the study of protoplanetary disks. In *European Physical Journal Web of Conferences*, volume 102 of *European Physical Journal Web of Conferences*, page 00009.

Ilee, J. D., Walsh, C., Booth, A. S., Aikawa, Y., Andrews, S. M., Bae, J., Bergin, E. A., Bergner, J. B., Bosman, A. D., Cataldi, G., Cleeves, L. I., Czekala, I., Guzmán, V. V., Huang, J., Law, C. J., Le Gal, R., Loomis, R. A., Ménard, F., Nomura, H., Öberg, K. I., Qi, C., Schwarz, K. R., Teague, R., Tsukagoshi, T., Wilner, D. J., Yamato, Y., and Zhang, K. (2021). Molecules with ALMA at Planet-forming Scales (MAPS). IX. Distribution and Properties of the Large Organic Molecules HC_3N, CH_3CN, and c-C_3H_2. *ApJS*, 257(1):9.

Isella, A., Huang, J., Andrews, S. M., Dullemond, C. P., Birnstiel, T., Zhang, S., Zhu, Z., Guzmán, V. V., Pérez, L. M., Bai, X.-N., Benisty, M., Carpenter, J. M., Ricci, L., and Wilner, D. J. (2018). The Disk Substructures at High Angular Resolution Project (DSHARP). IX. A High-definition Study of the HD 163296 Planet-forming Disk. *ApJL*, 869(2):L49.

Johansen, A., Blum, J., Tanaka, H., Ormel, C., Bizzarro, M., and Rickman, H. (2014). The Multifaceted Planetesimal Formation Process. In Beuther, H., Klessen, R. S., Dullemond, C. P., and Henning, T., editors, *Protostars and Planets VI*, pages 547–570.

Kamp, I., Thi, W. F., Woitke, P., Rab, C., Bouma, S., and Ménard, F. (2017). Consistent dust and gas models for protoplanetary disks. II. Chemical networks and rates. *AAp*, 607:A41.

Kamp, I., Tilling, I., Woitke, P., Thi, W. F., and Hogerheijde, M. (2010). Radiation thermochemical models of protoplanetary disks. II. Line diagnostics. *AAp*, 510:A18.

Kanwar, J., Kamp, I., Woitke, P., Rab, C., Thi, W. F., and Min, M. (2024). Hydrocarbon chemistry in the inner regions of planet-forming disks. *AAp*, 681:A22.

Krijt, S., Ciesla, F. J., and Bergin, E. A. (2016). Tracing Water Vapor and Ice During Dust Growth. *ApJ*, 833(2):285.

Law, C. J., Loomis, R. A., Teague, R., Öberg, K. I., Czekala, I., Andrews, S. M., Huang, J., Aikawa, Y., Alarcón, F., Bae, J., Bergin, E. A., Bergner, J. B., Boehler, Y., Booth, A. S., Bosman, A. D., Calahan, J. K., Cataldi, G., Cleeves, L. I., Furuya, K., Guzmán, V. V., Ilee, J. D., Le Gal, R., Liu, Y., Long, F., Ménard, F., Nomura, H., Qi, C., Schwarz, K. R., Sierra, A., Tsukagoshi, T., Yamato, Y., van't Hoff, M. L. R., Walsh, C., Wilner, D. J., and Zhang, K. (2021). Molecules with ALMA at Planet-forming Scales (MAPS). III. Characteristics of Radial Chemical Substructures. *ApJS*, 257(1):3.

Le Gal, R., Öberg, K. I., Teague, R., Loomis, R. A., Law, C. J., Walsh, C., Bergin, E. A., Ménard, F., Wilner, D. J., Andrews, S. M., Aikawa, Y., Booth, A. S., Cataldi, G., Bergner, J. B., Bosman, A. D., Cleeves, L. I., Czekala, I., Furuya, K., Guzmán, V. V., Huang, J., Ilee, J. D., Nomura, H., Qi, C., Schwarz, K. R., Tsukagoshi, T., Yamato, Y., and Zhang, K. (2021).

Molecules with ALMA at Planet-forming Scales (MAPS). XII. Inferring the C/O and S/H Ratios in Protoplanetary Disks with Sulfur Molecules. *ApJS*, 257(1):12.

Lissauer, J. J. (1993). Planet formation. *ARAA*, 31:129–174.

Liu, Y., Dipierro, G., Ragusa, E., Lodato, G., Herczeg, G. J., Long, F., Harsono, D., Boehler, Y., Menard, F., Johnstone, D., Pascucci, I., Pinilla, P., Salyk, C., van der Plas, G., Cabrit, S., Fischer, W. J., Hendler, N., Manara, C. F., Nisini, B., Rigliaco, E., Avenhaus, H., Banzatti, A., and Gully-Santiago, M. (2019). Ring structure in the MWC 480 disk revealed by ALMA. *AAp*, 622:A75.

Long, F., Pinilla, P., Herczeg, G. J., Harsono, D., Dipierro, G., Pascucci, I., Hendler, N., Tazzari, M., Ragusa, E., Salyk, C., Edwards, S., Lodato, G., van de Plas, G., Johnstone, D., Liu, Y., Boehler, Y., Cabrit, S., Manara, C. F., Menard, F., Mulders, G. D., Nisini, B., Fischer, W. J., Rigliaco, E., Banzatti, A., Avenhaus, H., and Gully-Santiago, M. (2018). Gaps and Rings in an ALMA Survey of Disks in the Taurus Star-forming Region. *ApJ*, 869(1):17.

Ma, R., Quan, D., Zhou, Y., Esimbek, J., Li, D., Li, X., Zhang, X., Tuo, J., and Feng, Y. (2024). Investigating Sulfur Chemistry in the HD 163296 disk. *arXiv e-prints*, page arXiv:2406.07896.

Madhusudhan, N., Harrington, J., Stevenson, K. B., Nymeyer, S., Campo, C. J., Wheatley, P. J., Deming, D., Blecic, J., Hardy, R. A., Lust, N. B., Anderson, D. R., Collier-Cameron, A., Britt, C. B. T., Bowman, W. C., Hebb, L., Hellier, C., Maxted, P. F. L., Pollacco, D., and West, R. G. (2011). A high C/O ratio and weak thermal inversion in the atmosphere of exoplanet WASP-12b. *nat*, 469(7328):64–67.

Madhusudhan, N., Sarkar, S., Constantinou, S., Holmberg, M., Piette, A. A. A., and Moses, J. I. (2023). Carbon-bearing Molecules in a Possible Hycean Atmosphere. *ApJL*, 956(1):L13.

Meijerink, R., Pontoppidan, K. M., Blake, G. A., Poelman, D. R., and Dullemond, C. P. (2009). Radiative Transfer Models of Mid-Infrared H_2O Lines in the Planet-Forming Region of Circumstellar Disks. *ApJ*, 704(2):1471–1481.

Monnier, J. D. (2003). Optical interferometry in astronomy. *Reports on Progress in Physics*, 66(5):789–857.

Najita, J. R., Ádámkovics, M., and Glassgold, A. E. (2011). Formation of Organic Molecules and Water in Warm Disk Atmospheres. *ApJ*, 743(2):147.

Öberg, K. I., Facchini, S., and Anderson, D. E. (2023). Protoplanetary Disk Chemistry. *ARAA*, 61:287–328.

Öberg, K. I., Guzmán, V. V., Walsh, C., Aikawa, Y., Bergin, E. A., Law, C. J., Loomis, R. A., Alarcón, F., Andrews, S. M., Bae, J., Bergner, J. B., Boehler, Y., Booth, A. S., Bosman, A. D., Calahan, J. K., Cataldi, G., Cleeves, L. I., Czekala, I., Furuya, K., Huang, J., Ilee, J. D., Kurtovic, N. T., Le Gal, R., Liu, Y., Long, F., Ménard, F., Nomura, H., Pérez, L. M., Qi, C., Schwarz, K. R., Sierra, A., Teague, R., Tsukagoshi, T., Yamato, Y., van't Hoff, M. L. R., Waggoner, A. R., Wilner, D. J., and Zhang, K. (2021). Molecules with ALMA at Planet-forming Scales (MAPS). I. Program Overview and Highlights. *ApJS*, 257(1):1.

Öberg, K. I., Murray-Clay, R., and Bergin, E. A. (2011). The Effects of Snowlines on C/O in Planetary Atmospheres. *ApJL*, 743(1):L16.

Parker, R., Ward-Thompson, D., and Kirk, J. (2022). Taxonomy of protoplanetary discs observed with ALMA. *MNRAS*, 511(2):2453–2490.

Rohatgi, A. (2024). Webplotdigitizer: Version 5. https://automeris.io/WebPlotDigitizer.

Stolker, T., Dominik, C., Avenhaus, H., Min, M., de Boer, J., Ginski, C., Schmid, H. M., Juhasz, A., Bazzon, A., Waters, L. B. F. M., Garufi, A., Augereau, J. C., Benisty, M., Boccaletti, A., Henning, T., Langlois, M., Maire, A. L., Ménard, F., Meyer, M. R., Pinte, C., Quanz, S. P., Thalmann, C., Beuzit, J. L., Carbillet, M., Costille, A., Dohlen, K., Feldt, M., Gisler, D., Mouillet, D., Pavlov, A., Perret, D., Petit, C., Pragt, J., Rochat, S., Roelfsema, R., Salasnich, B., Soenke, C., and Wildi, F. (2016). Shadows cast on the transition disk of HD 135344B. Multiwavelength VLT/SPHERE polarimetric differential imaging. *AAp*, 595:A113.

Teague, R. (2019). Gofish: Fishing for line observations in protoplanetary disks. *The Journal of Open Source Software*, 4(41):1632.

Thi, W. F., Woitke, P., and Kamp, I. (2011). Radiation thermo-chemical models of protoplanetary discs - III. Impact of inner rims on spectral energy distributions. *MNRAS*, 412(2):711–726.

Waters, L. B. F. M. and Waelkens, C. (1998). Herbig Ae/Be Stars. *ARAA*, 36:233–266.

Wichittanakom, C., Oudmaijer, R. D., Fairlamb, J. R., Mendigutía, I., Vioque, M., and Ababakr, K. M. (2020). The accretion rates and mechanisms of Herbig Ae/Be stars. *MNRAS*, 493(1):234–249.

Williams, J. P. and Cieza, L. A. (2011). Protoplanetary Disks and Their Evolution. *ARAA*, 49(1):67–117.

Woitke, P., Kamp, I., Antonellini, S., Anthonioz, F., Baldovin-Saveedra, C., Carmona, A., Dionatos, O., Dominik, C., Greaves, J., Güdel, M., Ilee, J. D., Liebhardt, A., Menard, F., Min, M., Pinte, C., Rab, C., Rigon, L., Thi, W. F., Thureau, N., and Waters, L. B. F. M. (2019). Consistent Dust and Gas Models for Protoplanetary Disks. III. Models for Selected Objects from the FP7 DIANA Project. *pasp*, 131(1000):064301.

Woitke, P., Kamp, I., and Thi, W. F. (2009). Radiation thermo-chemical models of protoplanetary disks. I. Hydrostatic disk structure and inner rim. *AAp*, 501(1):383–406.

Woitke, P., Min, M., Pinte, C., Thi, W. F., Kamp, I., Rab, C., Anthonioz, F., Antonellini, S., Baldovin-Saavedra, C., Carmona, A., Dominik, C., Dionatos, O., Greaves, J., Güdel, M., Ilee, J. D., Liebhart, A., Ménard, F., Rigon, L., Waters, L. B. F. M., Aresu, G., Meijerink, R., and Spaans, M. (2016). Consistent dust and gas models for protoplanetary disks. I. Disk shape, dust settling, opacities, and PAHs. *AAp*, 586:A103.

Zhang, K., Booth, A. S., Law, C. J., Bosman, A. D., Schwarz, K. R., Bergin, E. A., Öberg, K. I., Andrews, S. M., Guzmán, V. V., Walsh, C., Qi, C., van't Hoff, M. L. R., Long, F., Wilner, D. J., Huang, J., Czekala, I., Ilee, J. D., Cataldi, G., Bergner, J. B., Aikawa, Y., Teague, R., Bae, J., Loomis, R. A., Calahan, J. K., Alarcón, F., Ménard, F., Le Gal, R., Sierra, A., Yamato, Y., Nomura, H., Tsukagoshi, T., Pérez, L. M., Trapman, L., Liu, Y., and Furuya, K. (2021). Molecules with ALMA at Planet-forming Scales (MAPS). V. CO Gas Distributions. *ApJS*, 257(1):5.